Biomedicine & Pharmacotherapy 140 (2021) 111738

Contents lists available at ScienceDirect

Biomedicine & Pharmacotherapy

journal homepage: www.elsevier.com/locate/biopha

Original article

The sodium-glucose cotransporter-2 inhibitor Tofogliflozin prevents the progression of nonalcoholic steatohepatitis–associated liver tumors in a novel murine model

Naoki Yoshioka [a,d,1], Miyako Tanaka [a,e,*,1], Kozue Ochi [a], Akiko Watanabe [a], Kenji Ono [b,f], Makoto Sawada [b,f], Tomoo Ogi [c,g], Michiko Itoh [a,i], Ayaka Ito [a,e], Yukihiro Shiraki [h], Atsushi Enomoto [h], Masatoshi Ishigami [d], Mitsuhiro Fujishiro [d], Yoshihiro Ogawa [a,j], Takayoshi Suganami [a,e,*]

[a] Department of Molecular Medicine and Metabolism, Research Institute of Environmental Medicine, Nagoya University, Nagoya, Japan
[b] Department of Brain Function, Research Institute of Environmental Medicine, Nagoya University, Nagoya, Japan
[c] Department of Genetics, Research Institute of Environmental Medicine, Nagoya University, Nagoya, Japan
[d] Department of Gastroenterology and Hepatology, Nagoya University Graduate School of Medicine, Nagoya, Japan
[e] Department of Immunometabolism, Nagoya University Graduate School of Medicine, Nagoya, Japan
[f] Department of Molecular Pharmacokinetics, Nagoya University Graduate School of Medicine, Nagoya, Japan
[g] Department of Human Genetics and Molecular Biology, Nagoya University Graduate School of Medicine, Nagoya, Japan
[h] Department of Pathology, Nagoya University Graduate School of Medicine, Nagoya, Japan
[i] Kanagawa Institute of Industrial Science and Technology, Ebina, Japan
[j] Department of Medicine and Bioregulatory Science, Graduate School of Medical Sciences, Kyushu University, Fukuoka, Japan

ARTICLE INFO

Keywords:
Diabetes
Nonalcoholic steatohepatitis
Hepatocellular carcinoma
Animal model
Sodium glucose cotransporter 2 inhibitor
Cellular senescence

ABSTRACT

Background: Diabetes and obesity contribute to the pathogenesis of nonalcoholic steatohepatitis (NASH) and hepatocellular carcinoma (HCC). However, how diabetes and obesity accelerate liver tumorigenesis remains to be fully understood. Moreover, to verify the therapeutic potential of anti-diabetic drugs, there exists a strong need for appropriate animal models that recapitulate human pathophysiology of NASH and HCC.
Methods: We established a novel murine model of NASH-associated liver tumors using genetically obese melanocortin 4 receptor-deficient mice fed on Western diet in combination with a chemical procarcinogen, and verified the validity of our model in evaluating drug efficacy.
Findings: Our model developed multiple liver tumors together with obesity, diabetes, and NASH within a relatively short period (approximately 3 months). In this model, sodium glucose cotransporter 2 inhibitor Tofogliflozin prevented the development of NASH-like liver phenotypes and the progression of liver tumors. Tofogliflozin attenuated p21 expression of hepatocytes in non-tumorous lesions in the liver.
Interpretation: Tofogliflozin treatment attenuates cellular senescence of hepatocytes under obese and diabetic conditions. This study provides a unique animal model of NASH-associated liver tumors, which is applicable for assessing drug efficacy to prevent or treat NASH-associated HCC.

1. Introduction

Growing evidence has suggested that diabetes and obesity approximately doubles the risk of developing hepatocellular carcinoma (HCC) [1,2]. Nonalcoholic fatty liver disease (NAFLD) is a hepatic phenotype of the metabolic syndrome, and the progressive form, nonalcoholic steatohepatitis (NASH), increases the risk of cirrhosis and HCC [3]. Recent meta-analyses estimate the global prevalence of diabetes among patients with NAFLD and NASH at 23% and 44%, respectively [4]. Thus, there is a consensus that diabetes and obesity are involved in the pathogenesis of NASH and HCC. In terms of the underlying mechanism, recent studies using animal models have pointed to the role of

* Corresponding authors at: Department of Molecular Medicine and Metabolism, Research Institute of Environmental Medicine, Nagoya University, Nagoya, Japan.
E-mail addresses: tanaka@riem.nagoya-u.ac.jp (M. Tanaka), suganami@riem.nagoya-u.ac.jp (T. Suganami).
[1] Naoki Yoshioka and Miyako Tanaka contributed equally to this work.

https://doi.org/10.1016/j.biopha.2021.111738

Available online 21 May 2021

proinflammatory cytokines, insulin and insulin-like growth factors, and metabolic stresses including lipotoxicity [5]. Obesity also induces liver tumorigenesis through gut microbiota dysbiosis [6]. However, how diabetes and obesity accelerate the development of NASH and HCC remains to be fully elucidated. Thus, there exists a strong need for appropriate animal models that recapitulate human pathophysiology of NASH and HCC. However, a large number of animal models require genetic modification in the liver, non-physiological nutrition, and a long duration to develop NASH and liver tumors.

The melanocortin 4 receptor (*Mc4r*), which is highly expressed in the hypothalamus of the brain, is implicated in the regulation of food intake and energy expenditure. *Mc4r* mutations are the most frequent monogenic cause of obesity, and *Mc4r* variants are associated with obesity in humans [7]. It is also known that *Mc4r*-deficient (*Mc4r* KO) mice exhibit morbid obesity with dysregulated glucose and lipid metabolism [8]. Recently, we have developed a murine model of NASH-associated liver tumors, in which *Mc4r* KO mice fed a Western diet (WD) sequentially developed hepatic steatosis, NASH, and multiple liver tumors. [9] Histological and transcriptomic analyses revealed that the liver tumors in *Mc4r* KO mice fed WD recapitulate the features of HCC in patients with NAFLD [9,10]. Nevertheless, there was a technical limitation that almost 1 year is required to develop liver tumors in this animal model.

There is currently no approved medication for the treatment of NASH. Besides the therapeutic approach specific for NASH, increasing attention has been paid to the therapeutic potential of anti-diabetic drugs for NASH and HCC. Among others, substantial evidence indicates that sodium glucose cotransporter 2 (SGLT2) inhibitors significantly improve hepatic steatosis in diabetic animals and diabetic patients with NAFLD, in addition to ameliorating blood glucose levels [11–13]. In terms of the potential mechanisms, SGLT2 inhibitors reduce the insulin-to-glucagon ratio and promote a shift from hepatic carbohydrate to fatty acid metabolism, resulting in reduction of the hepatic triglyceride content [14]. Moreover, we and other researchers reported that SGLT2 inhibitors are capable of preventing the development of liver tumors in obese diabetic mice [12,15]. However, only limited information is available about the effect of SGLT2 inhibitors on the development of HCC in patients with NAFLD.

In this study, we established a novel murine model of NASH-associated liver tumors using *Mc4r* KO mice fed WD in combination with a chemical procarcinogen, diethylnitrosamine (DEN). Our model developed multiple liver tumors together with obesity, diabetes, and NASH within a relatively short period (approximately 3 months). Using this model, we demonstrated that the SGLT2 inhibitor Tofogliflozin prevented the development of NASH-like liver phenotypes and the progression of liver tumors. In terms of the underlying mechanism, our data suggest that Tofogliflozin treatment attenuates cellular senescence of hepatocytes under obese and diabetic conditions. This study provides a unique animal model of NASH-associated liver tumors, which is applicable for assessing drug efficacy.

2. Research design and methods

2.1. Materials

All reagents were purchased from Sigma (St. Louis, MO) or Nacalai Tesque (Kyoto, Japan) unless otherwise specified. Tofogliflozin was provided by Kowa Company Ltd. (Nagoya, Japan).

2.2. Animals

Mc4r KO mice on the C57BL/6J background were kindly provided by Dr. Joel K. Elmquist (University of Texas Southwestern Medical Center) [16], and age-matched C57BL/6J wild-type mice were purchased from CLEA Japan (Tokyo, Japan). The animals were housed in a temperature-, humidity- and light-controlled animal room (with a 12-h light and 12-h dark cycle) and allowed free access to water and standard diet (CE-2; CLEA Japan). To induce liver tumors in a short duration, 2-week-old *Mc4r* KO mice received a single intraperitoneal injection of DEN (~25 mg/kg body weight) in saline, and the mice were fed WD (D12079B; 468 kcal/100 g, 41% energy as fat, 34.0% sucrose, 0.21% cholesterol; Research Diets, New Brunswick, NJ) from 6 weeks of age up to 14 weeks. For Tofogliflozin treatment, the mice received Tofogliflozin by oral gavage (5 mg/kg body weight/day) from 6 weeks of age. During the Tofogliflozin treatment period, pair-feeding was conducted to exclude the difference of caloric intake. The mice in the Tofogliflozin-treated group received the amount of food that was consumed by the mice in the control group on the day before. At the end of each experiment, the mice were sacrificed under deep anesthesia.

2.3. Blood parameters

Concentrations of blood glucose and serum insulin were measured on a blood glucose test meter (Glutest Mint; Sanwa Kagaku Kenkyusho, Nagoya, Japan) and a mouse insulin ELISA kit (Morinaga Institute of Biological Science, Kanagawa, Japan), respectively. Serum biochemical parameters were measured using DRI-CHEM NX500V (Fujifilm, Tokyo, Japan).

2.4. Hepatic lipid content

Total lipids in the liver were extracted with ice-cold 2:1 (vol/vol) chloroform/methanol. Hepatic triglyceride content was determined using triglyceride E-test Wako (FUJIFILM Wako Pure Chemical, Osaka, Japan).

2.5. Histological analysis

Liver samples were fixed with neutral-buffered formalin, embedded in paraffin, and cut into 2- and 4-μm-thick sections that were stained with hematoxylin and eosin and Sirius red, respectively [17]. Immunostainings for F4/80, Ki-67, cytokeratin 18, and p21 were performed as previously described [17], using anti-F4/80 (MCA497GA, Bio-Rad Laboratories, Hercules, CA), anti-Ki-67 (SP6, Novus Biologicals, Littleton, CO, USA), anti-cytokeratin 18 (NB100-79923, Novus Biologicals), and anti-p21 antibodies (ab188224, Abcam, Cambridge, UK), respectively. NAFLD activity score (NAS) was determined according to the published criteria [18]. Lobular inflammation and hepatocyte ballooning were identified as inflammatory foci scattered in the hepatic lobule and swollen hepatocytes with rarefied cytoplasm, respectively. Histological scoring and quantification were performed by hepatologists and pathologists in a blinded fashion.

2.6. Quantitative real-time PCR

Total RNA was extracted from the liver, kidney, and jejunum using the Sepasol reagent. Quantitative real-time PCR was performed with the StepOnePlus Real-time PCR System using a Fast SYBR Green Master Mix Reagent (Thermo Fisher Scientific, San Jose, CA) as described previously [17]. The primers used in this study are listed in Supplementary Table 1. Levels of mRNA were normalized to those of 36B4 mRNA.

2.7. Computed tomographic imaging

According to the manufacturer's instruction, mice under anesthesia were scanned using a computed tomography scanner, CosmoScan FX (Rigaku, Tokyo, Japan). The nonionic iodinated contrast agent iopamidol (Teva Takeda Pharma, Nagoya, Japan) was injected through the right external jugular vein with a dose of 0.5 ml/mouse, and the images were obtained during the portal venous and delayed phases.

2.8. Magnetic resonance imaging (MRI)

According to the manufacturer's instruction, mice under anesthesia were scanned using a 1.5-Tesla MRI scanner (MRmini SA 1508, DS Pharma Biomedical, Osaka, Japan). T1-weighted images (TR/TE of 500/9 ms, field of view of 30 mm, slice thickness of 2 mm) were acquired using an interleaving method. A dose of 0.1 mmol/kg body weight gadolinium ethoxybenzyl diethylenetriamine pentaacetic acid (Gd-EOB-DTPA) (Primovist, Bayer Schering Pharma, Berlin, Germany) was injected through the tail vein, and images were obtained during the hepatobiliary phase 15 min after the injection.

2.9. Statistical analysis

Data are presented as the mean ± SEM. P values < 0.05 were considered to be statistically significant. Statistical analysis was performed using analysis of variance, followed by Tukey's post hoc test for comparison between groups. Differences between two groups were analyzed using unpaired Student's t-test.

2.10. Study approval

All animal experiments were conducted in accordance with the guidelines for the care and use of laboratory animals of Nagoya University. The protocols were approved by the Animal Care and Use Committee, Research Institute of Environmental Medicine, Nagoya University (approval number: 20253).

3. Results

3.1. Mc4r deficiency in mice accelerates the development of DEN-induced liver tumors

To elucidate the effect of diabetic conditions on the development of liver tumors within a short duration, we sought to create a novel murine model of NASH-associated liver tumors. Given that obesity promotes chemically induced liver tumorigenesis [19,20], we conceived the combination of *Mc4r* KO mice and a chemical procarcinogen, DEN. First, three different doses (0, 1, and 25 mg/kg body weight) of DEN were injected intraperitoneally to 2-week-old *Mc4r* KO mice, and the mice were fed WD for 10 weeks from 6 weeks of age (Fig. 1a). DEN injection did not affect body weight, weights of epididymal fat and liver, or blood glucose levels in *Mc4r* KO mice (Fig. 1b). We confirmed that *Mc4r* KO mice with DEN injection did not develop liver tumors at 6 weeks of age (data not presented). In this experimental setting, most of the *Mc4r* KO mice receiving DEN injection developed liver tumors after 10 weeks of WD feeding, whereas *Mc4r* KO mice without DEN injection did not (Fig. 1c). The number of liver tumors was dependent on the doses of DEN (Fig. 1d), and the median size of the liver tumors was 2 mm in *Mc4r* KO mice receiving the high-dose DEN injection (Fig. 1e).

We next extended the period of WD feeding for up to 14 weeks (Fig. 1f). At this time point, we confirmed that *Mc4r* KO mice without DEN injection did not develop liver tumors (Fig. 1g). As expected, extension of the WD feeding period increased the number and size of liver tumors in *Mc4r* KO mice with DEN injection (Fig. 1h and i). We further examined the effects of *Mc4r* deficiency and WD feeding on the development of liver tumors. Wild-type mice fed WD and *Mc4r* KO mice fed a standard diet rarely developed liver tumors when they received DEN injection (Fig. 1j). Collectively, these results indicate that *Mc4r* deficiency in combination with WD feeding accelerates the development of DEN-induced liver tumors in mice.

3.2. Morphological features of DEN-induced liver tumors in Mc4r KO mice fed WD

Next, we sought to investigate the liver tumors in the accelerated model morphologically. In this study, *Mc4r* KO mice receiving DEN injection were fed WD for 12 weeks. Contrast-enhanced computed tomography (CECT) detected the liver tumors as isodense/hypodense nodular lesions in the portal venous and delayed phases (Fig. 2a). The tumors were also identified as hypointense nodules by Gd-EOB-DTPA-enhanced MRI in the hepatobiliary phase, because Gd-EOB-DTPA is taken up specifically by normal hepatocytes (Fig. 2a). These observations are compatible with those of dysplastic nodules and HCC in humans [21]. We further conducted histological examinations of the tumors. The tumors exhibited increased cell densities and an exophytic growth pattern, accompanied by the compression of the surrounding hepatic parenchyma. (Fig. 2b). It was noted that the tumor cells at the rims exhibited nuclei with mildly condensed chromatin with eosinophilic cytoplasm, suggesting that they recapitulate the features of human dysplastic nodules, Interestingly, a small number of the tumors exhibited larger size with cytological and architectural atypia, and minimal invasion into the stroma (Fig. 2c), which resembles the features of human well-differentiated HCC. The proportion of Ki-67-positive cells was higher in tumorous lesions compared to that in non-tumorous lesions (Fig. 2d), further indicating their proliferative capacity. Thus, the liver tumors developed in our model were histologically graded as tumors with low malignant potential that recapitulate human dysplastic nodules or well-differentiated HCC. These data, together with the above findings that the tumors were detected by the imaging modalities, further extended the utility of this model as a tool to study human NASH and HCC encountered in clinical practice.

3.3. DEN injection does not affect NASH-like liver phenotypes in Mc4r KO mice fed WD

We next evaluated the non-tumorous lesions of the liver in this model. As reported previously [9,22], *Mc4r* KO mice fed WD exhibited hepatic lipid accumulation and histological features compatible with human NASH, such as steatosis, lobular inflammation, hepatocyte ballooning, and peri-cellular fibrosis (Fig. 3a). Ballooned hepatocytes showed complete loss of cytokeratin 18 immunostaining. The NAS was approximately 5.7 at this time point (Fig. 3b). We previously reported that CLS (crown-like structure: a unique histological structure in the liver from experimental NASH models and human NASH, where dead hepatocytes with large lipid droplets are surrounded by macrophages) [22] serves as an origin of hepatic inflammation and fibrosis during the progression from simple steatosis to NASH [23]. In this study, DEN injection did not affect these histological features (Fig. 3b–d). In addition, we assessed mRNA expression of the genes related to inflammation (*Emr1* (F4/80, a macrophage marker), *Tnfa*, and *Il6*) and fibrosis (*Acta2* (α-smooth muscle actin) and *Tgfb1*) in non-tumorous lesions in the liver (Fig. 3e). In non-tumorous lesions, most of these mRNA levels were not affected by DEN injection. These results suggest that DEN injection does not affect NASH-like liver phenotypes in *Mc4r* KO mice fed WD.

3.4. Tofogliflozin ameliorates NASH-like liver phenotypes in Mc4r KO mice fed WD

Next, we verified the validity of our NASH-associated liver tumor model in evaluating drug efficacy. Tofogliflozin, an SGLT2 inhibitor, was orally administered to DEN-injected *Mc4r* KO mice fed WD for 12 weeks (Fig. 4a). During the Tofogliflozin treatment period, pair-feeding was conducted to exclude the difference of caloric intake between the groups (Fig. 4a and Supplementary Fig. 1). As expected, the Tofogliflozin-treated group had less body weight gain than the control group, along with lower blood glucose levels, and serum insulin concentrations (Fig. 4b and c). Tofogliflozin treatment also significantly reduced liver weight, the hepatic triglyceride content, and serum concentrations of aspartate aminotransferase (AST), alanine aminotransaminase (ALT), and lactate dehydrogenase (LDH) (Fig. 4d and Table 1), suggesting amelioration of hepatic steatosis. Histological

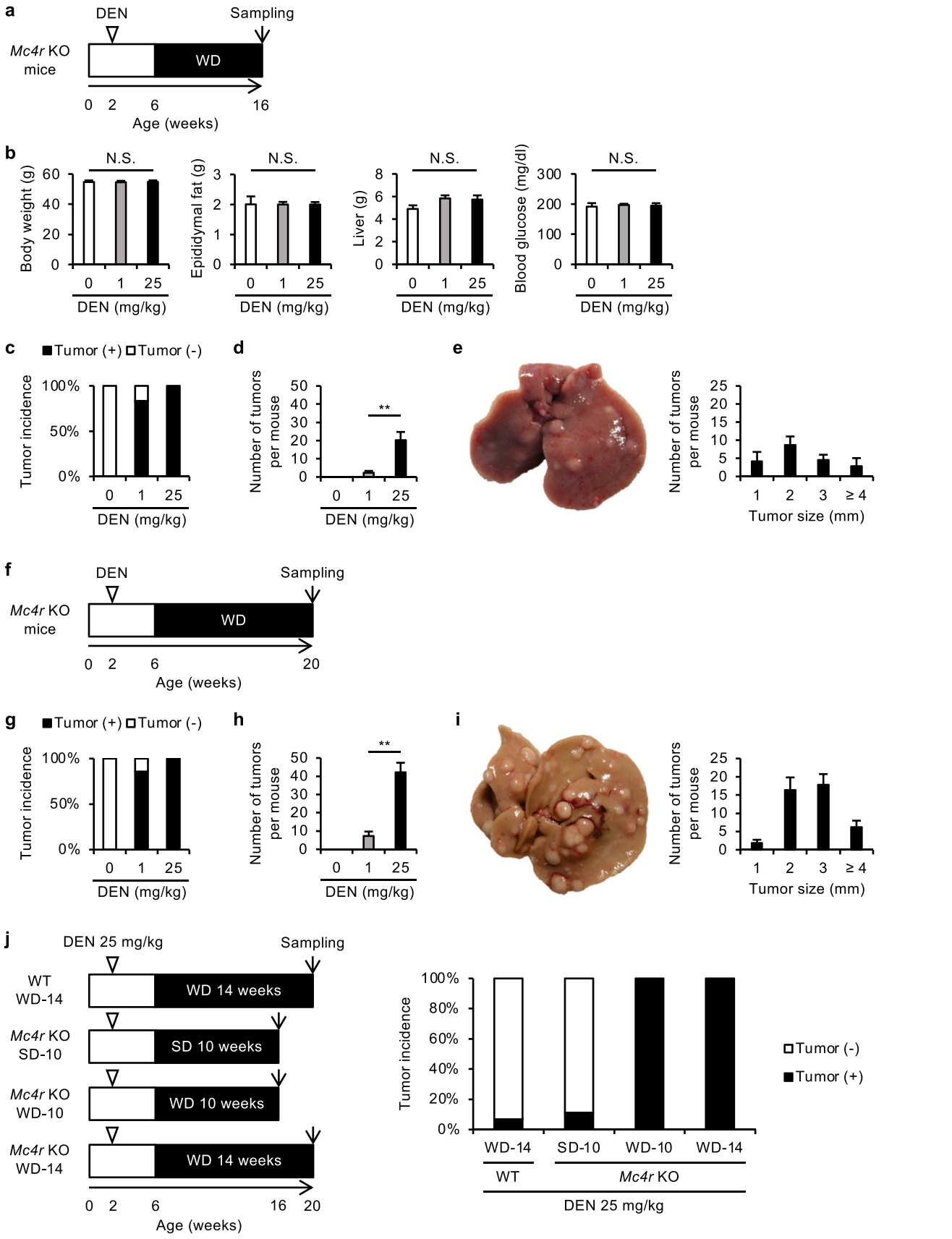

(caption on next page)

Fig. 1. *Mc4r* deficiency in mice accelerates the development of DEN-induced liver tumors. (a) Experimental protocol. Melanocortin 4 receptor-deficient (*Mc4r* KO) mice were injected intraperitoneally with different doses of diethylnitrosamine (DEN) at 2 weeks of age, and the mice fed Western diet (WD) for 10 weeks from 6 weeks of age. ($n = 6$) (b) Body weight, weights of epididymal fat and liver, and blood glucose levels. (c and d) Tumor incidence (c) and tumor multiplicity (d) after 10 weeks of WD feeding. (e) Representative image of gross appearance and size distribution of liver tumors in *Mc4r* KO mice. The mice were injected intraperitoneally with DEN (25 mg/kg body weight) and fed WD for 10 weeks. (f) Experimental protocol. *Mc4r* KO mice were injected intraperitoneally with different doses of DEN at 2 weeks of age, and the mice fed WD for 14 weeks from 6 weeks of age. ($n = 5$–7) (g and h) Tumor incidence (g) and tumor multiplicity (h) after 14 weeks of WD feeding. (i) Representative image of gross appearance and size distribution of liver tumors in *Mc4r* KO mice. The mice were injected intraperitoneally with DEN (25 mg/kg body weight) and fed WD for 14 weeks. (j) Experimental protocol to investigate the effect of *Mc4r* deficiency and WD feeding on liver tumorigenesis (*left*). Wild-type (WT) mice fed WD for 14 weeks ($n = 15$), *Mc4r* KO mice fed standard diet (SD) for 10 weeks ($n = 9$), *Mc4r* KO mice fed WD for 10 weeks ($n = 6$), and *Mc4r* KO mice fed WD for 14 weeks ($n = 6$). Tumor incidence of the 4 groups (*right*). Data represent mean ± SEM. $^{**}P < 0.01$. N.S. indicates not significant.

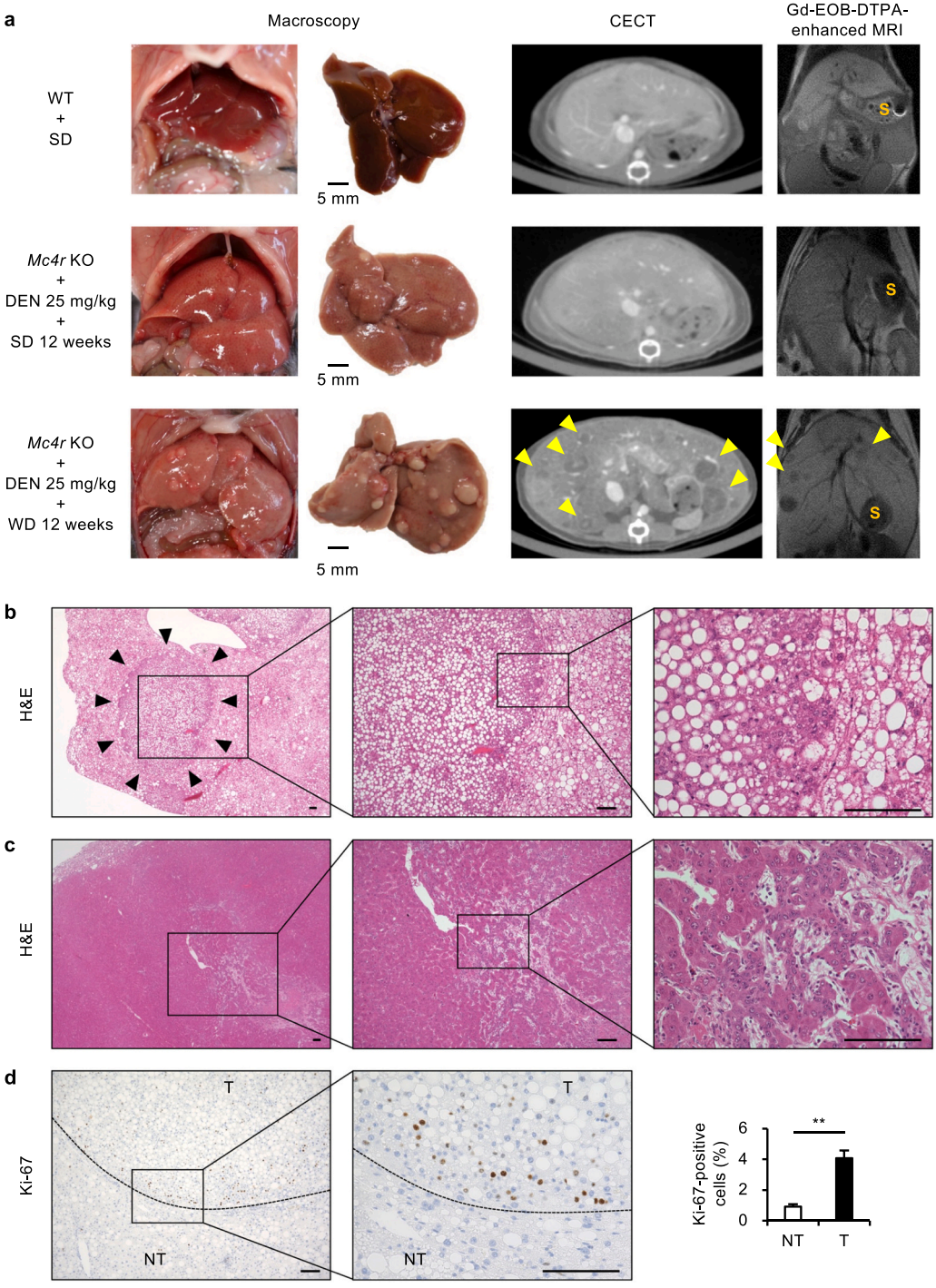

Fig. 2. Morphological features of DEN-induced liver tumors in *Mc4r* KO mice fed WD. (a) Representative images of gross appearance, contrast-enhanced computed tomography (CECT), and gadolinium ethoxybenzyl diethylenetriamine pentaacetic acid (Gd-EOB-DTPA)-enhanced magnetic resonance imaging (MRI) of the livers from WT and *Mc4r* KO mice. Arrowheads indicate liver tumors. S indicates stomach. (b and c) Representative images of hematoxylin and eosin (H&E) staining of the liver from DEN-injected *Mc4r* KO mice fed WD for 12 weeks. (b) Representative small ($\leq$ 1 mm in diameter) and (c) large ($\geq$ 2 mm in diameter) tumors. Scale bars, 100 μm. (d) Representative images of Ki-67 immunostaining of the liver from DEN-injected *Mc4r* KO mice fed WD for 12 weeks (*left*). Quantification of Ki-67-positive cells (*right*). The dotted line indicates the boundary between the tumorous (T) and non-tumorous (NT) lesions. Scale bars, 100 μm. Data represent mean ± SEM. $n = 8$. $^{**}P < 0.01$.

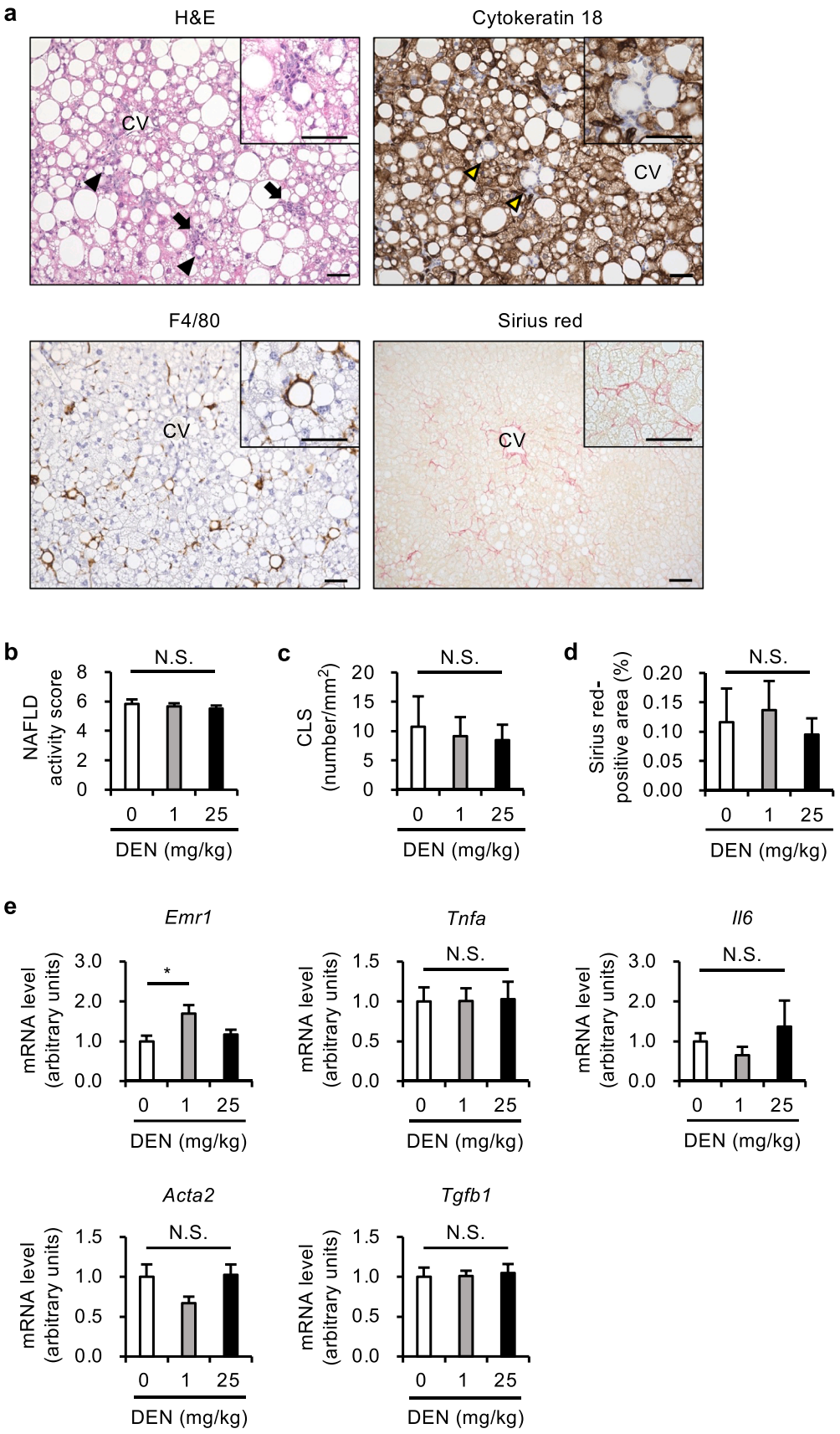

Fig. 3. DEN injection does not affect NASH-like liver phenotypes in *Mc4r* KO mice fed WD. (a) Representative images of H&E staining, cytokeratin 18 and F4/80 immunostaining, and Sirius red staining in non-tumorous lesions of the liver from DEN-injected *Mc4r* KO mice fed WD for 10 weeks. CV, central vein. Scale bars, 50 μm. Arrows and arrowheads indicate lobular inflammation and hepatocyte ballooning, respectively. Insets in the H&E and cytokeratin 18 panels indicate representative images of hepatocyte ballooning. Insets in the F4/80 and Sirius red panels indicate representative images of crown-like structure (CLS) and peri-cellular fibrosis, respectively. (b–d) Quantification of NAFLD activity score (b), the number of CLS (c), and Sirius red-positive area (d). (e) Expression levels of genes related to inflammation (F4/80 (*Emr1*), tumor necrosis factor-α (*Tnfa*), and interleukin-6 (*Il6*)), and fibrosis (α-smooth muscle actin (*Acta2*) and tumor growth factor-β1 (*Tgfb1*)) in non-tumorous lesions of the liver. Data represent mean ± SEM. $n = 6$. $^*P < 0.05$. N.S. indicates not significant.

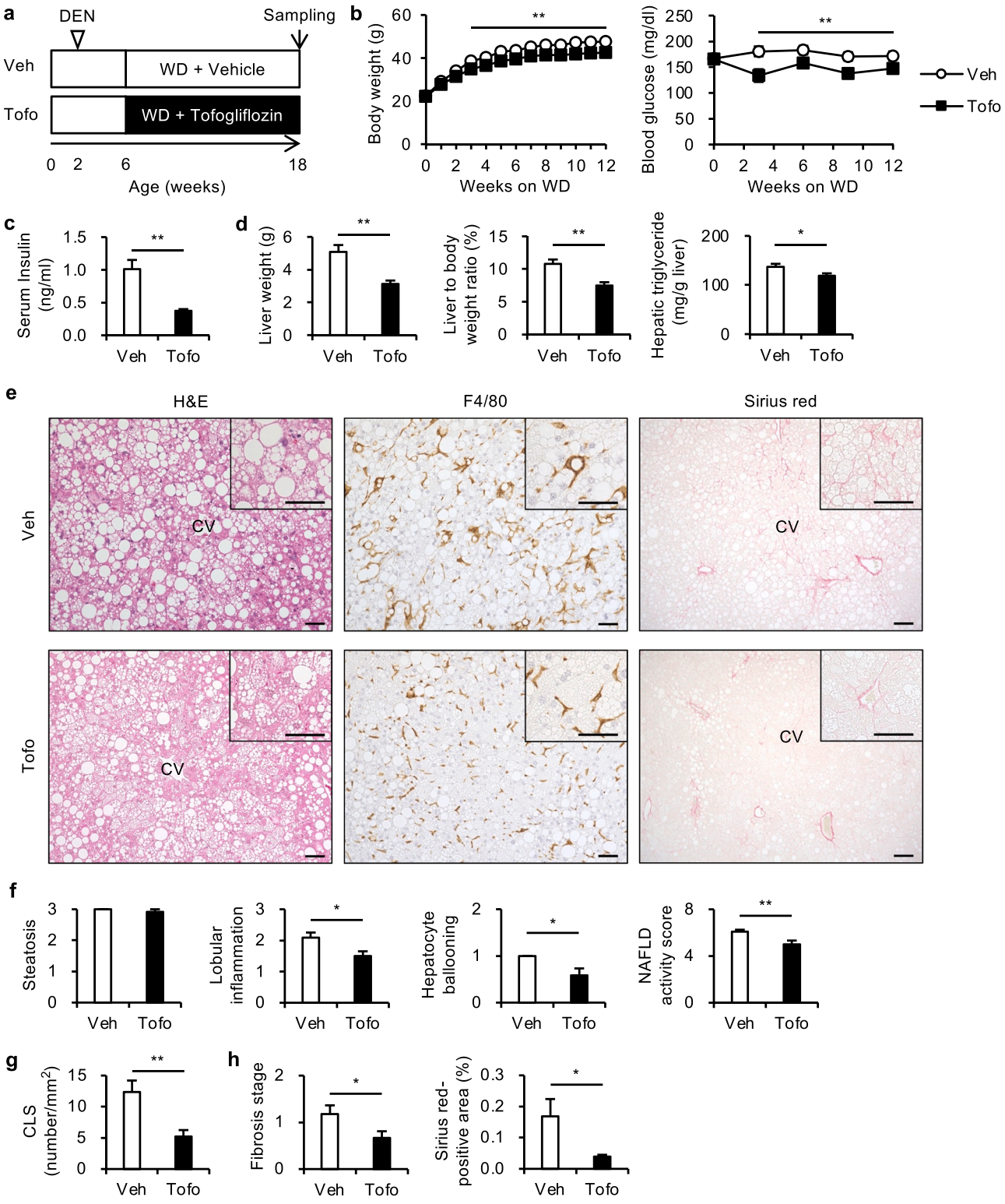

Fig. 4. Tofogliflozin ameliorates NASH-like liver phenotypes in *Mc4r* KO mice fed WD. (a) Experimental protocol. *Mc4r* KO mice were injected intraperitoneally with DEN (25 mg/kg body weight) at 2 weeks of age, and the mice fed WD from 6 weeks of age for 12 weeks. Vehicle (Veh) or Tofogliflozin (Tofo) was orally administered to DEN-injected *Mc4r* KO mice when they were fed WD. The mice in the Tofogliflozin-treated group received the amount of food that was consumed by the mice in the control vehicle-treated group on the day before. (b) Time course of body weight and blood glucose levels. (c and d) Serum insulin concentrations (c), liver weight, and hepatic triglyceride content (d) after 12 weeks of WD feeding. (e) Representative images of H&E staining, F4/80 immunostaining, and Sirius red staining of the liver after 12 weeks of WD feeding. Scale bars, 50 μm. CV, central vein. Insets in each panel indicate representative images of hepatocyte ballooning, crown-like structure (CLS), and peri-cellular fibrosis. (f–h) Quantification of NAFLD activity score (f), the number of CLS (g), and Sirius red-positive area (h). Data represent mean ± SEM. Veh, $n = 11$; Tofo, $n = 12$. $^{*}P < 0.05$, $^{**}P < 0.01$.

Table 1
Metabolic parameters of DEN-injected *Mc4r* KO mice fed WD with or without Tofogliflozin treatment.

	Vehicle	Tofogliflozin
Body wight (g)	46.59 ± 1.00	41.80 ± 0.38**
Epididymal fat weight (g)	1.73 ± 0.09	1.70 ± 0.05
Epididymal fat to body weight ratio (%)	3.74 ± 0.21	4.06 ± 0.11
AST (U/l)	247.73 ± 13.87	151.25 ± 16.15**
ALT (U/l)	304.27 ± 22.00	172.00 ± 27.94**
LDH (U/l)	1224.55 ± 83.23	775.83 ± 94.94**
Serum total cholesterol (mg/dl)	330.82 ± 19.36	289.58 ± 21.89
Serum triglyceride (mg/dl)	80.91 ± 5.34	70.50 ± 3.54

DEN, diethylnitrosamine; WD, Western diet. Data represent mean ± SEM.
**$P < 0.01$ vs. Vehicle. Vehicle, $n = 11$; Tofogliflozin, $n = 12$.

examination of non-tumorous lesions revealed that there was a significant reduction in NAS in the Tofogliflozin-treated group compared to that in the control group (Fig. 4e and f). Moreover, Tofogliflozin treatment markedly reduced CLS formation and hepatic fibrosis (Fig. 4e, g, and h). These results, taken together, indicate that Tofogliflozin treatment prevents inflammation and fibrosis in the liver associated with hepatic lipid accumulation and systemic diabetic conditions in *Mc4r* KO mice fed WD.

3.5. Tofogliflozin prevents the progression of NASH-associated liver tumors

We further analyzed whether Tofogliflozin is capable of preventing NASH-associated liver tumorigenesis utilizing DEN-injected *Mc4r* KO mice fed WD. Although there was no significant difference in the proportion of the mice developing liver tumors between both groups, the number of tumors tended to be less in the Tofogliflozin-treated group relative to that in the control group (Fig. 5a and b). In particular, the number of large tumors ($\geq$ 2 mm in diameter) was significantly less in the Tofogliflozin-treated group (Fig. 5b). To elucidate the underlying mechanism, we compared mRNA expression of the genes related to cell proliferation in tumorous lesions between both groups. We found that there was only a slight decrease in *Pcna* and *Bax* mRNA levels in the Tofogliflozin-treated group (Fig. 5c), which does not seem to have a strong impact on liver tumorigenesis. We also examined mRNA expression of the genes related to tumor survival such as cell senescence, glucose and lipid metabolism, and tumor-associated macrophages, but there was no appreciable difference between the two groups (Fig. 5d–f). In addition, mRNA levels of *Sglt1* and *Sglt2* were almost negligible in tumorous lesions (Supplementary Fig. 2), suggesting that Tofogliflozin does not directly act on the tumors in our model. These results led us to speculate that Tofogliflozin exerts its anti-tumor effects through the non-tumorous lesions of the liver.

3.6. Tofogliflozin inhibits cellular senescence in non-tumorous lesions of the liver

As previously described [11], Tofogliflozin treatment affected mRNA expression of the genes related to glucose and lipid metabolism, in which the β-oxidation and gluconeogenic pathways were upregulated, and the lipogenic pathway was downregulated (Fig. 6a). Tofogliflozin treatment also decreased mRNA expression of the genes related to inflammation and fibrosis (Fig. 6b). These observations are consistent with the preventive effect of Tofogliflozin on inflammation and fibrosis in the liver of DEN-injected *Mc4r* KO mice fed WD (Fig. 4). Notably, we found that mRNA expression of the genes related to a senescence-associated secretory phenotype (SASP), such as *p21*, *Cxcl1*, *Mmp12*, and *Mmp13*, was significantly reduced by Tofogliflozin treatment (Fig. 6c). Of note, WD feeding and *Mc4r* deficiency increased mRNA levels of these genes, whereas DEN injection did not change these mRNA levels in the non-tumorous lesions of the liver in *Mc4r* KO mice fed WD, (Supplementary Figs. 3 and 4). Then, we focused on p21, a key regulator of cellular senescence, because accumulating evidence has pointed to the pathological role of cellular senescence in the development of NASH and HCC [24]. Histological examination revealed that most of the p21-positive cells were hepatocytes and that the number of p21-positive hepatocytes was significantly decreased by Tofogliflozin treatment (Fig. 6d). These results indicate that Tofogliflozin treatment ameliorates cellular senescence of hepatocytes during the progression of NASH in *Mc4r* KO mice fed WD, which may underlie the preventive effect of Tofogliflozin on the progression of liver tumors.

4. Discussion

To date, a large number of animal models have been introduced to investigate the molecular link by which diabetes and obesity accelerate NASH-associated HCC. However, recapitulating human pathophysiology in animal models remains a challenge. Indeed, a large number of animal models require genetic modification in the liver, non-physiological nutrition, and a long duration to develop NASH and liver tumors. In this study, we propose a novel murine model of NASH-associated HCC using WD-fed *Mc4r* KO mice in combination with DEN injection. DEN is metabolized to DNA alkylating agents by cytochrome P450 enzymes specifically in hepatocytes [25]. The introduction of oncogenic mutations into hepatocytes during normal post-natal development then results in liver tumors. Park et al. reported that dietary and genetic obesity promote DEN-induced liver tumorigenesis [19]. This model requires a relatively long duration (approximately 1 year) to develop liver tumors and exhibits simple hepatic steatosis but not NASH. Our model developed NASH and multiple liver tumors within a relatively short period (approximately 3 months), together with obesity and diabetes. Of note, *Mc4r* KO mice fed a standard diet and wild-type mice fed WD exhibited simple hepatic steatosis only and did not develop liver tumors when they received DEN injection. These findings are consistent with the recent epidemiological data indicating that NASH possesses a much higher risk for HCC than simple hepatic steatosis: the annual incidence of HCC in patients with NASH is 5.29 per 1000 persons, whereas that in patients with NAFLD is 0.44 per 1000 persons [4]. In addition, it should be highlighted that *Mc4r* is predominantly expressed in the brain and rarely in the liver, and thus our model is distinguished from other models with genetic manipulations within the liver. Accordingly, our model would be a unique animal model for investigating the molecular mechanisms underlying the progression of NASH-associated HCC.

There is substantial evidence that diabetes is involved in the pathogenesis of NASH and HCC. However, the underlying mechanism is complex and remains to be elucidated [26]. Accumulating evidence suggests that hyperinsulinemia and insulin resistance cause hepatic lipid accumulation [27,28], resulting in lipotoxicity. In addition to the aberrant metabolism, liver inflammation and ongoing regeneration during the progression to NASH contribute to DNA instability and then tumorigenesis [29]. In this study, we focused on cellular senescence in hepatocytes as one of the mechanisms. Recent evidence has pointed to the involvement of hepatocyte cellular senescence in the pathogenesis of both NASH and HCC. For instance, lipid accumulation activates the p53-p21 and p16-Rb pathways in hepatocytes of animals and patients with NAFLD [30–32], and hepatocyte p21 expression is positively correlated with fibrosis stage and glycemic control [32]. The fundamental role of hepatocyte senescence is to limit excessive or aberrant cellular proliferation and thus protect against tumorigenesis. On the other hand, Aravinthan et al. reported that cellular senescence in hepatocytes is associated with the adverse liver-related outcome including HCC in humans [32]. This is probably because efficient clearance of senescent hepatocytes is indispensable in this process [33,34]. In this regard, WD feeding and *Mc4r* deficiency increased hepatic mRNA expression of SASP factors whereas DEN injection did not affect their mRNA levels. Tofogliflozin treatment attenuated cellular senescence of

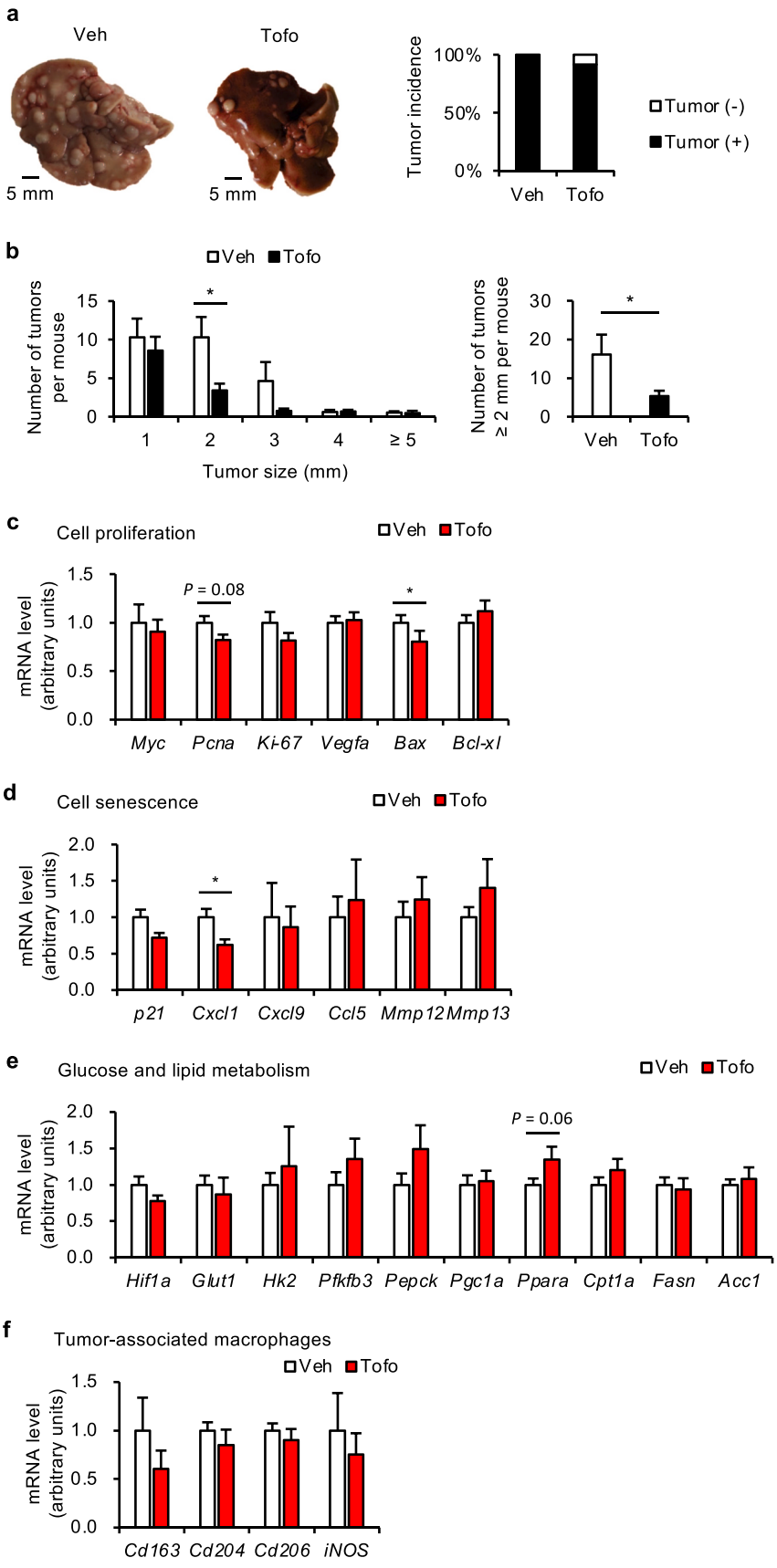

Fig. 5. Tofogliflozin prevents the progression of NASH-associated liver tumors. (a) Representative images of gross appearance of liver tumors and tumor incidence in DEN-injected *Mc4r* KO mice fed WD for 12 weeks. Veh, $n = 11$; Tofo, $n = 12$. (b) Size distribution of liver tumors. (c–f) Expression levels of genes related to cell proliferation (c), cellular senescence (d), glucose and lipid metabolism (e), and tumor-associated macrophages (f) in tumorous lesions. Veh, $n = 14$; Tofo, $n = 9$. Data represent mean ± SEM. $^*P < 0.05$.

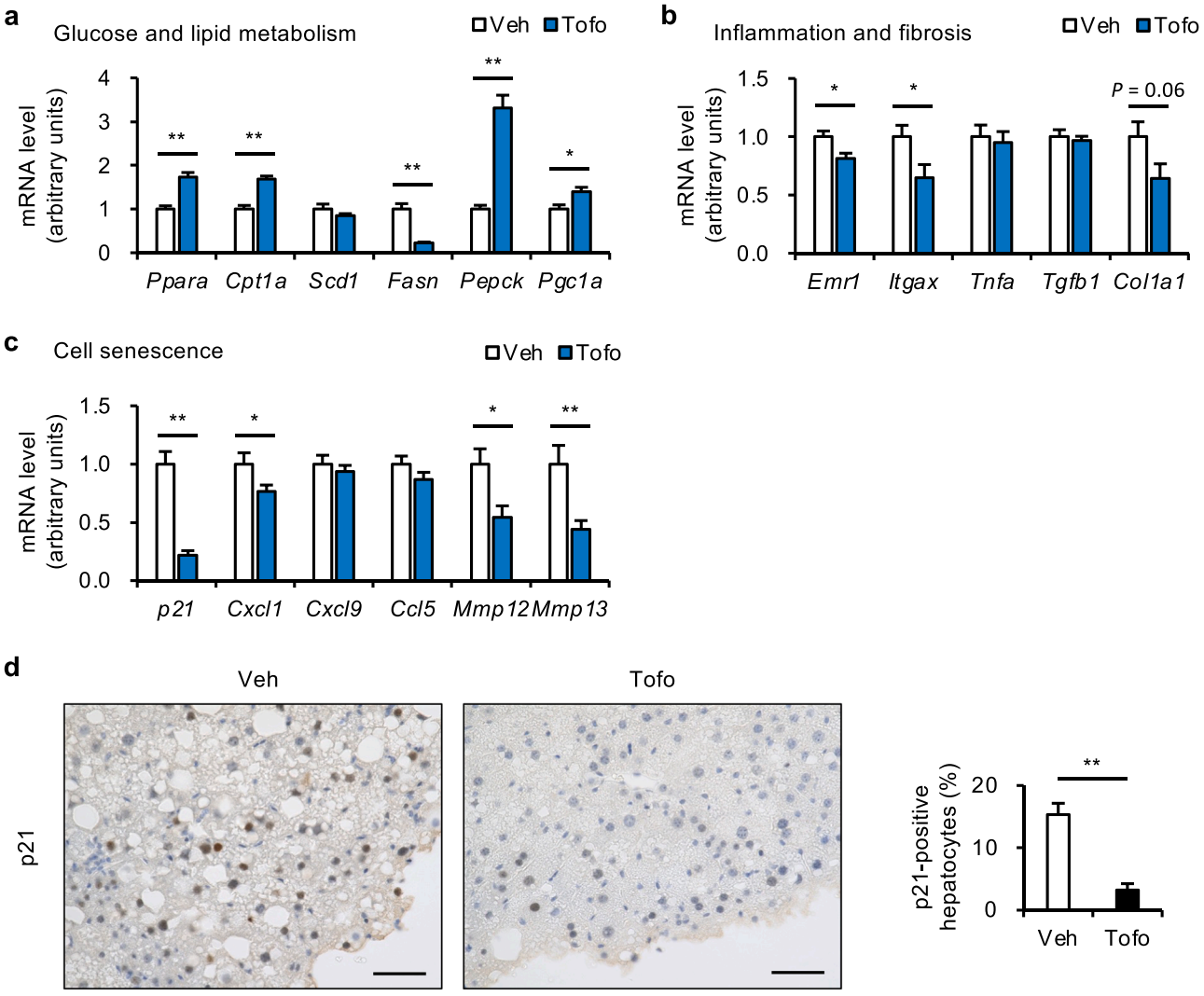

Fig. 6. Tofogliflozin inhibits cellular senescence in non-tumorous lesions of the liver. (a–c) Expression levels of genes related to glucose and lipid metabolism (a), inflammation and fibrosis (b), and cellular senescence (c) in non-tumorous lesions of the liver in DEN-injected *Mc4r* KO mice fed WD for 12 weeks. (d) Representative images of p21 immunostaining and the number of p21-positive hepatocytes. Scale bars, 50 μm. Data represent mean ± SEM. Veh, $n = 11$; Tofo, $n = 12$. $^{*}P < 0.05$, $^{**}P < 0.01$.

hepatocytes as well as histological features of NASH. Taken together, this study suggests that cellular senescence in hepatocytes accelerates DEN-induced liver tumorigenesis under diabetic and obese conditions.

In addition to hepatocytes, Tofogliflozin treatment may have affected stromal cells. Several studies previously reported that liver tumorigenesis is promoted not only by senescent hepatocytes but also cellular senescence in stromal cells such as hepatic stellate cells [20,35,36]. Of note, senescent hepatocytes potently induce cellular senescence in surrounding stromal cells by producing SASP factors [37]. Therefore, it is conceivable that Tofogliflozin treatment mitigates cellular senescence of hepatocytes and probably stromal cells, thus preventing the progression of liver tumors. Further studies are required to fully understand the effects of Tofogliflozin treatment in each cell type in the liver during the progression of liver tumors. In addition, from the clinical viewpoint, we need to elucidate the therapeutic effect of Tofogliflozin on already existing liver tumors in the future. Collectively, this study proves the validity of our model in testing drug efficacy for NASH and liver tumors.

We need to discuss the possible role of weight reduction in prevention of liver tumor progression following Tofogliflozin treatment. Substantial evidence demonstrates that weight loss improves histological features in human NASH [38,39]. Dietary restriction also protects against lipid accumulation and cellular senescence in the liver of aged mice [31]. Accordingly, we do not exclude the possibility that prevention of hepatocyte senescence, NASH-like liver phenotypes, and progression of liver tumors is attributed, at least in part, to reduced weight gain by Tofogliflozin treatment. Of note, recent studies have shown that SGLT2 inhibitors have novel mechanisms of action such as increased circulating levels of ketone bodies, in addition to weight loss and glycemic control [40].

Our study has several limitations. First, the molecular characteristics of DEN-induced liver tumors may be different from those of human HCC, despite the histopathological mimicry [41,42]. Most of the liver tumors in our model recapitulated dysplastic nodules in humans, and they could be detected by the modalities commonly used in clinical practice. Second, our model exhibits morbid obesity and severe insulin resistance, whereas patients with NASH-associated HCC are not necessarily diabetic and obese. Finally, we previously reported the preventive effect of the SGLT2 inhibitor Canagliflozin on the development of NASH and liver tumors using *Mc4r* KO mice fed WD for 1 year without DEN. Although SGLT2 inhibitors are analogous in their pharmacological properties, further studies are required to confirm the class effect. Since a recent clinical study revealed that improved glycemic control decreases the incidence of HCC after sero-clearance of a hepatitis B surface antigen in

patients with diabetes [43], understanding the mode of action of SGLT2 inhibitors in our model may be applicable for various types of HCC.

In conclusion, we established a novel murine model of NASH-associated liver tumors, which develops hepatic steatosis, NASH, and multiple liver tumors, along with obesity and diabetes, within a relatively short period. Utilizing this model, we also demonstrated that Tofogliflozin treatment effectively prevents the progression of NASH-associated liver tumors, probably by mitigating cellular senescence of hepatocytes. Thus, this study verifies the validity of our NASH model as a unique in vivo tool for assessing drug efficacy to prevent or treat NASH-associated HCC.

Funding

This work was supported in part by Grants-in-Aid for Scientific Research from the Ministry of Education, Culture, Sports, Science and Technology of Japan (20H03447, 20H05503, and 20H04944 to T.S. and 18K08508 to M.T.) and Japan Agency for Medical Research and Development (CREST) (JP20gm1210009s0102 to T.S.) and Research Program on Hepatitis (JP20fk0210082s0101 to T.S. and JP21fk0210094 to M.T.). This study was also supported by research grants from The Hori Sciences and Arts Foundation, Japan, DAIKO Foundation, Japan, Kobayashi Foundation, Japan, and Takeda Science Foundation, Japan (T.S.).

CRediT authorship contribution statement

M.T., T.S. study concept and design; **N.Y., M.T., Ko.O., A.W.** acquisition of data; **Mi.I., Ke.O., M.S., T.O.** analysis and interpretation of data; **N.Y., Y.S., A.E., Ma.I., M.F.** histological analysis; **N.Y., M.T., T.S.** drafting of the manuscript; **A.I., Y.O.** critical revision of the manuscript; **N.Y., M.T.** statistical analysis; **M.F., Y.O., T.S.** study supervision.

Acknowledgments

We thank Dr. Joel K. Elmquist (University of Texas Southwestern Medical Center) for his generous gift of MC4R-KO mice. We also thank Drs. Ayumu Taguchi and Yuichi Abe (Aichi Cancer Center) and the members of the Suganami laboratory for their helpful discussions, and Center for Animal Research and Education (CARE), Nagoya University for support on animal experiments.

Declaration of conflicting interests

No potential conflicts of interest relevant to this article were reported.

Appendix A. Supporting information

Supplementary data associated with this article can be found in the online version at doi:10.1016/j.biopha.2021.111738.

References

[1] H.B. El-Serag, H. Hampel, F. Javadi, The association between diabetes and hepatocellular carcinoma: a systematic review of epidemiologic evidence, Clin. Gastroenterol. Hepatol. 4 (2006) 369–380.
[2] S.C. Larsson, A. Wolk, Overweight, obesity and risk of liver cancer: a meta-analysis of cohort studies, Br. J. Cancer 97 (2007) 1005–1008.
[3] G.A. Michelotti, M.V. Machado, A.M. Diehl, NAFLD, NASH and liver cancer, Nat. Rev. Gastroenterol. Hepatol. 10 (2013) 656–665.
[4] Z.M. Younossi, A.B. Koenig, D. Abdelatif, Y. Fazel, L. Henry, M. Wymer, Global epidemiology of nonalcoholic fatty liver disease-meta-analytic assessment of prevalence, incidence, and outcomes, Hepatology 64 (2016) 73–84.
[5] R. Karagozian, Z. Derdák, G. Baffy, Obesity-associated mechanisms of hepatocarcinogenesis, Metabolism 63 (2014) 607–617.
[6] L.X. Yu, R.F. Schwabe, The gut microbiome and liver cancer: mechanisms and clinical translation, Nat. Rev. Gastroenterol. Hepatol. 14 (2017) 527–539.
[7] C. Vaisse, K. Clement, E. Durand, S. Hercberg, B. Guy-Grand, P. Froguel, Melanocortin-4 receptor mutations are a frequent and heterogeneous cause of morbid obesity, J. Clin. Investig. 106 (2000) 253–262.
[8] D.C. Albarado, J. McClaine, J.M. Stephens, R.L. Mynatt, J. Ye, A.W. Bannon, W. G. Richards, A.A. Butler, Impaired coordination of nutrient intake and substrate oxidation in melanocortin-4 receptor knockout mice, Endocrinology 145 (2004) 243–252.
[9] M. Itoh, T. Suganami, N. Nakagawa, M. Tanaka, Y. Yamamoto, Y. Kamei, S. Terai, I. Sakaida, Y. Ogawa, Melanocortin 4 receptor-deficient mice as a novel mouse model of nonalcoholic steatohepatitis, Am. J. Pathol. 179 (2011) 2454–2463.
[10] N. Chiyonobu, S. Shimada, Y. Akiyama, K. Mogushi, M. Itoh, K. Akahoshi, S. Matsumura, K. Ogawa, H. Ono, Y. Mitsunori, D. Ban, A. Kudo, S. Arii, T. Suganami, S. Yamaoka, Y. Ogawa, M. Tanabe, S. Tanaka, Fatty Acid Binding Protein 4 (FABP4) overexpression in intratumoral hepatic stellate cells within hepatocellular carcinoma with metabolic risk factors, Am. J. Pathol. 188 (2018) 1213–1224.
[11] A. Obata, N. Kubota, T. Kubota, M. Iwamoto, H. Sato, Y. Sakurai, I. Takamoto, H. Katsuyama, Y. Suzuki, M. Fukazawa, S. Ikeda, K. Iwayama, K. Tokuyama, K. Ueki, T. Kadowaki, Tofogliflozin improves insulin resistance in skeletal muscle and accelerates lipolysis in adipose tissue in male mice, Endocrinology 157 (2016) 1029–1042.
[12] K. Shiba, K. Tsuchiya, C. Komiya, Y. Miyachi, K. Mori, N. Shimazu, S. Yamaguchi, N. Ogasawara, M. Katoh, M. Itoh, T. Suganami, Y. Ogawa, Canagliflozin, an SGLT2 inhibitor, attenuates the development of hepatocellular carcinoma in a mouse model of human NASH, Sci. Rep. 8 (2018) 2362.
[13] G. Ranjbar, D.P. Mikhailidis, A. Sahebkar, Effects of newer antidiabetic drugs on nonalcoholic fatty liver and steatohepatitis: think out of the box!, Metabolism 101 (2019), 154001.
[14] E. Ferrannini, S. Baldi, S. Frascerra, B. Astiarraga, T. Heise, R. Bizzotto, A. Mari, T. R. Pieber, E. Muscelli, Shift to fatty substrate utilization in response to sodium-glucose cotransporter 2 inhibition in subjects without diabetes and patients with type 2 diabetes, Diabetes 65 (2016) 1190–1195.
[15] K. Obara, Y. Shirakami, A. Maruta, T. Ideta, T. Miyazaki, T. Kochi, H. Sakai, T. Tanaka, M. Seishima, M. Shimizu, Preventive effects of the sodium glucose cotransporter 2 inhibitor tofogliflozin on diethylnitrosamine-induced liver tumorigenesis in obese and diabetic mice, Oncotarget 8 (2017) 58353–58363.
[16] N. Balthasar, L.T. Dalgaard, C.E. Lee, J. Yu, H. Funahashi, T. Williams, M. Ferreira, V. Tang, R.A. McGovern, C.D. Kenny, L.M. Christiansen, E. Edelstein, B. Choi, O. Boss, C. Aschkenasi, C.Y. Zhang, K. Mountjoy, T. Kishi, J.K. Elmquist, B. B. Lowell, Divergence of melanocortin pathways in the control of food intake and energy expenditure, Cell 123 (2005) 493–505.
[17] M. Kawakubo, M. Tanaka, K. Ochi, A. Watanabe, M. Saka-Tanaka, Y. Kanamori, N. Yoshioka, S. Yamashita, M. Goto, M. Itoh, I. Shirakawa, S. Kanai, H. Suzuki, M. Sawada, A. Ito, M. Ishigami, M. Fujishiro, H. Arima, Y. Ogawa, T. Suganami, Dipeptidyl peptidase-4 inhibition prevents nonalcoholic steatohepatitis-associated liver fibrosis and tumor development in mice independently of its anti-diabetic effects, Sci. Rep. 10 (2020) 983.
[18] D.E. Kleiner, E.M. Brunt, M. Van Natta, C. Behling, M.J. Contos, O.W. Cummings, L. D. Ferrell, Y.C. Liu, M.S. Torbenson, A. Unalp-Arida, M. Yeh, A.J. McCullough, A. J. Sanyal, N. Nonalcoholic Steatohepatitis Clinical Research, Design and validation of a histological scoring system for nonalcoholic fatty liver disease, Hepatology 41 (2005) 1313–1321.
[19] E.J. Park, J.H. Lee, G.Y. Yu, G. He, S.R. Ali, R.G. Holzer, C.H. Osterreicher, H. Takahashi, M. Karin, Dietary and genetic obesity promote liver inflammation and tumorigenesis by enhancing IL-6 and TNF expression, Cell 140 (2010) 197–208.
[20] S. Yoshimoto, T.M. Loo, K. Atarashi, H. Kanda, S. Sato, S. Oyadomari, Y. Iwakura, K. Oshima, H. Morita, M. Hattori, K. Honda, Y. Ishikawa, E. Hara, N. Ohtani, Obesity-induced gut microbial metabolite promotes liver cancer through senescence secretome, Nature 499 (2013) 97–101.
[21] A. Forner, J.M. Llovet, J. Bruix, Hepatocellular carcinoma, Lancet 379 (2012) 1245–1255.
[22] M. Itoh, H. Kato, T. Suganami, K. Konuma, Y. Marumoto, S. Terai, H. Sakugawa, S. Kanai, M. Hamaguchi, T. Fukaishi, S. Aoe, K. Akiyoshi, Y. Komohara, M. Takeya, I. Sakaida, Y. Ogawa, Hepatic crown-like structure: a unique histological feature in non-alcoholic steatohepatitis in mice and humans, PLoS One 8 (2013) 82163.
[23] M. Itoh, T. Suganami, H. Kato, S. Kanai, I. Shirakawa, T. Sakai, T. Goto, M. Asakawa, I. Hidaka, H. Sakugawa, K. Ohnishi, Y. Komohara, K. Asano, I. Sakaida, M. Tanaka, Y. Ogawa, CD11c+ resident macrophages drive hepatocyte death-triggered liver fibrosis in a murine model of nonalcoholic steatohepatitis, JCI Insight 2 (2017), e92902.
[24] A.M. Papatheodoridi, L. Chrysavgis, M. Koutsilieris, A. Chatzigeorgiou, The role of senescence in the development of nonalcoholic fatty liver disease and progression to nonalcoholic steatohepatitis, Hepatology 71 (2020) 363–374.
[25] L. Verna, J. Whysner, G.M. Williams, N-nitrosodiethylamine mechanistic data and risk assessment: bioactivation, DNA-adduct formation, mutagenicity, and tumor initiation, Pharmacol. Ther. 71 (1996) 57–81.
[26] H. Tilg, A.R. Moschen, M. Roden, NAFLD and diabetes mellitus, Nat. Rev. Gastroenterol. Hepatol. 14 (2017) 32–42.
[27] G. Marchesini, M. Brizi, G. Bianchi, S. Tomassetti, E. Bugianesi, M. Lenzi, A. J. McCullough, S. Natale, G. Forlani, N. Melchionda, Nonalcoholic fatty liver disease: a feature of the metabolic syndrome, Diabetes 50 (2001) 1844–1850.
[28] K.M. Utzschneider, A. Van de Lagemaat, M.V. Faulenbach, J.H. Goedecke, D. B. Carr, E.J. Boyko, W.Y. Fujimoto, S.E. Kahn, Insulin resistance is the best predictor of the metabolic syndrome in subjects with a first-degree relative with type 2 diabetes, Obesity 18 (2010) 1781–1787.

[29] Q.M. Anstee, H.L. Reeves, E. Kotsiliti, O. Govaere, M. Heikenwalder, From NASH to HCC: current concepts and future challenges, Nat. Rev. Gastroenterol. Hepatol. 16 (2019) 411–428.
[30] X. Zhang, D. Zhou, R. Strakovsky, Y. Zhang, Y.X. Pan, Hepatic cellular senescence pathway genes are induced through histone modifications in a diet-induced obese rat model, Am. J. Physiol. Gastrointest. Liver Physiol. 302 (2012) G558–G564.
[31] M. Ogrodnik, S. Miwa, T. Tchkonia, D. Tiniakos, C.L. Wilson, A. Lahat, C.P. Day, A. Burt, A. Palmer, Q.M. Anstee, S.N. Grellscheid, J. Hoeijmakers, S. Barnhoorn, D. A. Mann, T.G. Bird, W.P. Vermeij, J.L. Kirkland, J.F. Passos, T. von Zglinicki, D. Jurk, Cellular senescence drives age-dependent hepatic steatosis, Nat. Commun. 8 (2017) 15691.
[32] A. Aravinthan, C. Scarpini, P. Tachtatzis, S. Verma, S. Penrhyn-Lowe, R. Harvey, S. E. Davies, M. Allison, N. Coleman, G. Alexander, Hepatocyte senescence predicts progression in non-alcohol-related fatty liver disease, J. Hepatol. 58 (2013) 549–556.
[33] W. Xue, L. Zender, C. Miething, R.A. Dickins, E. Hernando, V. Krizhanovsky, C. Cordon-Cardo, S.W. Lowe, Senescence and tumour clearance is triggered by p53 restoration in murine liver carcinomas, Nature 445 (2007) 656–660.
[34] T.W. Kang, T. Yevsa, N. Woller, L. Hoenicke, T. Wuestefeld, D. Dauch, A. Hohmeyer, M. Gereke, R. Rudalska, A. Potapova, M. Iken, M. Vucur, S. Weiss, M. Heikenwalder, S. Khan, J. Gil, D. Bruder, M. Manns, P. Schirmacher, F. Tacke, M. Ott, T. Luedde, T. Longerich, S. Kubicka, L. Zender, Senescence surveillance of pre-malignant hepatocytes limits liver cancer development, Nature 479 (2011) 547–551.
[35] A. Krtolica, S. Parrinello, S. Lockett, P.Y. Desprez, J. Campisi, Senescent fibroblasts promote epithelial cell growth and tumorigenesis: a link between cancer and aging, Proc. Natl. Acad. Sci. USA 98 (2001) 12072–12077.
[36] S. Parrinello, J.P. Coppe, A. Krtolica, J. Campisi, Stromal-epithelial interactions in aging and cancer: senescent fibroblasts alter epithelial cell differentiation, J. Cell Sci. 118 (2005) 485–496.
[37] J.C. Acosta, A. Banito, T. Wuestefeld, A. Georgilis, P. Janich, J.P. Morton, D. Athineos, T.W. Kang, F. Lasitschka, M. Andrulis, G. Pascual, K.J. Morris, S. Khan, H. Jin, G. Dharmalingam, A.P. Snijders, T. Carroll, D. Capper, C. Pritchard, G. J. Inman, T. Longerich, O.J. Sansom, S.A. Benitah, L. Zender, J. Gil, A complex secretory program orchestrated by the inflammasome controls paracrine senescence, Nat. Cell Biol. 15 (2013) 978–990.
[38] K. Promrat, D.E. Kleiner, H.M. Niemeier, E. Jackvony, M. Kearns, J.R. Wands, J. L. Fava, R.R. Wing, Randomized controlled trial testing the effects of weight loss on nonalcoholic steatohepatitis, Hepatology 51 (2010) 121–129.
[39] E. Vilar-Gomez, Y. Martinez-Perez, L. Calzadilla-Bertot, A. Torres-Gonzalez, B. Gra-Oramas, L. Gonzalez-Fabian, S.L. Friedman, M. Diago, M. Romero-Gomez, Weight loss through lifestyle modification significantly reduces features of nonalcoholic steatohepatitis, Gastroenterology 149 (2015) 367–378, 367–78.e5.
[40] M.R. Cowie, M. Fisher, SGLT2 inhibitors: mechanisms of cardiovascular benefit beyond glycaemic control, Nat. Rev. Cardiol. 17 (2020) 761–772.
[41] F. Connor, T.F. Rayner, S.J. Aitken, C. Feig, M. Lukk, J. Santoyo-Lopez, D.T. Odom, Mutational landscape of a chemically-induced mouse model of liver cancer, J. Hepatol. 69 (2018) 840–850.
[42] M. Dow, R.M. Pyke, B.Y. Tsui, L.B. Alexandrov, H. Nakagawa, K. Taniguchi, E. Seki, O. Harismendy, S. Shalapour, M. Karin, H. Carter, J. Font-Burgada, Integrative genomic analysis of mouse and human hepatocellular carcinoma, Proc. Natl. Acad. Sci. USA 115 (2018) E9879–E9888.
[43] T. Cheuk-Fung Yip, V. Wai-Sun Wong, H. Lik-Yuen Chan, Y.K. Tse, A. Pik-Shan Kong, K. Long-Yan Lam, G. Chung-Yan Lui, G. Lai-Hung Wong, Effects of diabetes and glycemic control on risk of hepatocellular carcinoma after seroclearance of hepatitis b surface antigen, Clin. Gastroenterol. Hepatol. 16 (2018) 765–773, 765–773.e762.